Biomolecular NMR Assignments (2023) 17:17–22
https://doi.org/10.1007/s12104-022-10113-3

ARTICLE

^{1}H, ^{13}C and ^{15}N assignment of the human mitochondrial paramagnetic iron–sulfur protein CISD3

José Malanho Silva[1] · Deborah Grifagni[1] · Francesca Cantini[1,2] · Mario Piccioli[1,2]

Received: 13 September 2022 / Accepted: 25 November 2022 / Published online: 15 December 2022

Abstract

CISD3 is a mitochondrial protein that contains two [2Fe–2S] clusters. This protein is overexpressed in some types of cancer, so it has emerged as a potential drug target. A detailed characterization of this protein is crucial to understand how CISD3 is involved in these physiopathologies. In this study, isotopically labeled human CISD3 was expressed in *Escherichia coli*. A set of double and triple resonance experiments performed with standard parameters/datasets provided the assignment of 40% of the HN resonances, 47% of Cα, and 46% of C′ resonances. Tailored paramagnetic HSQC, CON and CACO experiments extended up to 59% for HN, 70% for Cα and 69% for C′. The ^{1}H, ^{13}C and ^{15}N NMR chemical shift assignment of human CISD3 is reported here.

Keywords CISD3 · Iron–sulfur clusters · Paramagnetic NMR

Biological context

Iron–sulfur (Fe–S) clusters are essential protein cofactors and are involved in a wide variety of cell functions, such as catalysis, electron transport and environmental sensing. The CISD3 protein (also known as MiNT or Miner2) has 127 amino acids and is present in the mitochondria, however its specific location inside the mitochondria remains unknown. This protein has two 2Fe–2S clusters, and each cluster is coordinated by 3Cys:1His in a conserved motif domain (CDGSH). To date, there only exists one structure of a mutant construct of CISD3 where the two 2Fe–2S clusters are coordinated by 4Cys (PDB code 6AVJ) and the N-terminus is removed (Lipper et al. 2018). The 1–14 residues N-terminal fragment contains the sequence for a signal peptide to transport the protein to the mitochondria and is predicted to be highly unstructured (Lipper et al. 2018).

Human CISD3 protein has a single polypeptide chain containing a four-stranded beta-cap that connects both CDGSH domains followed by a short alpha helix segment. The CDGSH domain is a loop region that contains the three Cys residues responsible for coordinating the FeS centers and the short alpha helix contains the FeS coordinating His residues.

The function of CISD3 remains elusive, however previous studies related this protein to cancer (Li et al. 2021; Lipper et al. 2018). Furthermore, since CISD3 has homology to the other two NEET proteins, it also may be involved in aging (Chen et al. 2009), diabetes (Ferecatu et al. 2014; Kusminski et al. 2012) and neurodegenerative diseases (He et al. 2016; Mittler et al. 2019; Salameh et al. 2021). To investigate the mechanism of action of this protein as well the potential as a drug target, we took the challenge to assign the NMR signals of this highly paramagnetic protein. We performed the assignment of the WT form of the protein in which the N-term fragment has been removed. The [2Fe–2S] clusters shuttle between the +2/+1 oxidation states; the oxidized forms contains two Fe^{3+} ions that are antiferromagnetically coupled while the reduced state contains one Fe^{3+} and one Fe^{2+} ion. We report here the study of the protein in its fully reduced form, in which both clusters are in the reduced $[2Fe–2S]^{+}$ state.

✉ Mario Piccioli
piccioli@cerm.unifi.it

[1] Magnetic Resonance Center and Department of Chemistry, University of Florence, Via L. Sacconi 6, 50019 Sesto Fiorentino, Italy

[2] Consorzio Interuniversitario Risonanze Magnetiche Metalloproteine, Via L. Sacconi 6, 50019 Sesto Fiorentino, Italy

Methods and experiments

Expression and purification protocol

The CISD3 gene (37–127 preceded by a methionine and a glycine) was inserted into a pET28a(+) plasmid, resulting in a construct with 93 residues. The plasmid was used to transform E. coli BL21 (DE3) gold competent cells. Cell growth was performed in M9 (3.0 g ^{13}C-D-glucose and 1.2 g $^{15}NH_4Cl$ per litre) medium by adding 4 cm^3 of Q solution and 500 µM Mohr's Salt at 37 °C. When the culture reached an OD 600 of 0.8–1, 0.1 mM IPTG was added to induce protein overexpression, and the cells were incubated at 18 °C overnight. All the purification steps were performed in anaerobic environment. Cells were resuspended in 80 cm^3 of 20 mM Tris-HCl, pH 7.5 degassed buffer and lysed by adding CelLytic Reagent (0.8 g × 1 L culture) and it was incubated for 20 min. After incubation the lysate was diluted up to 200 cm^3, filtered using a 0.22 µm filter and then loaded in a HiTrap SP FF cationic exchange column. The column was washed with a step NaCl gradient until CISD3 protein solution eluted with 20 mM Tris-HCl pH 7.5 and 300 mM NaCl. The final NMR sample had a protein concentration of 500 µM in 20 mM Tris-HCl, 300 mM NaCl, 2 mM dithiothreitol (DTT) pH 7.5 and 10% (v/v) D_2O.

NMR spectroscopy for backbone assignment

All NMR experiments used for resonance assignment for the reduced CISD3 were recorded on a Bruker AVANCE 700 MHz spectrometer on 0.5 mM ^{13}C-^{15}N-labeled samples in a buffered solution with 20 mM Tris-HCl, 300 mM NaCl, 2 mM DTT, pH 7.5 and 10% (v/v) D_2O. All NMR spectra were collected at 298 K, processed using the standard Bruker software Topspin and analyzed through the CARA program (Keller 2004).For the backbone resonance assignments of diamagnetic signals, we recorded ^{1}H detected ^{15}N- and ^{13}C-HSQC, HNCA, HNCO, HNCOCA, CBCACONH and ^{13}C detected CACO and CON. For this set of experiments, radio frequency pulses, carrier frequencies, acquisition and processing parameters were taken as normally done in biomolecular NMR studies.

The CACO experiment was recorded using a ^{1}H start experiment with a CT evolution in the Cα dimension (Bermel et al. 2008). Furthermore, to identify signals affected by paramagnetic relaxation, we performed double and triple resonance experiments using parameters optimized to identify signals with high R_1 and R_2 values (Trindade et al. 2021b). A ^{15}N HSQC-AP spectrum (Ciofi-Baffoni et al. 2014) was acquired, with 512 scans/fid, using INEPT and recycle delays of 714 us and 0.25 s, respectively. Acquisition times were shortened to 47 ms (t2) and 27 ms (t1). CACO and CON experiments optimized to identify fast relaxing signals were also recorded. For the CACO experiment we recorded a paramagnetic version of the ^{1}H start CACO experiment using 0.7 ms for the Hα-Cα and 2.7 ms for the Cα-C^O INEPT transfer delays. 1024 experiments were collected using acquisition times of 46 ms (t_2) and 4 ms (t_1), with a recycle delay of 0.4 s. During Cα evolution, the constant time period was removed, at variance with the experiment optimized for the identification of diamagnetic signals. A ^{13}C start experiment was also recorded using a CACO-AP experiment (Bertini et al. 2005). 1024 scans for each fid were recorded with CACO INEPT delay of 2.7 ms, a recycle delay of 0.3 s and acquisition times of 24.6 ms (t_2) and 7.6 ms (t_1). For the paramagnetic version of the CON experiment, we recorded 1024 scans over 128 increments, using acquisition times of 28 ms (t_2) and 19.2 ms (t_1), with a C^O–N INEPT delay of 8 ms and a recycle delay of 0.2 s. Proton resonances were calibrated with respect to the signal of 2,2-dimethylsilapentane-5-sulfonic acid (DSS). Nitrogen chemical shifts were referenced indirectly to the ^{1}H standard using a conversion factor derived from the ratio of NMR frequencies. Carbon resonances were calibrated using the signal of dioxane at 69.4 ppm (298 K) as secondary reference.

^1H_N-relaxation experiments

Measurements of ^{1}HN R_1 and R_2 relaxation rates were carried out using 11.7 T Bruker AVANCE 500 equipped with a triple resonance, inverse detection, cryoprobe (TXI). ^1H_N relaxation measurements rates, both diamagnetic and paramagnetic, were recorded at 298 K at 500 MHz, using a protein concentration of 0.5 mM. The In-Phase (IP) experiments were acquired with recycle delays of 2 s, while the Anti-Phase (AP) experiments were acquired with recycle delays of 150 ms. Typically, R_1 values > 10 s^{-1} and R_2 values > 50 s^{-1} were taken from the AP experiments, lower rates were measured with the IP experiments.

A series of thirteen ^{1}HN-R_1 ^{15}N-HSQC-IP experiments were recorded using a transfer INEPT period of 0.001 s, 0.01 s, 0.02 s, 0.05 s, 0.08 s, 0.12 s, 0.16 s, 0.2 s, 0.3 s, 0.5 s, 0.7 s, 1 s and 1.8 s. For each experiment, 32 scans were collected over 128 increments.

A series of thirteen ^{1}HN-R_1-weighted ^{15}N-HSQC-AP experiments was recorded, using INEPT transfer periods of 2 ms, 4 ms, 6 ms, 10 ms, 15 ms, 20 ms, 25 ms, 30 ms, 40 ms, 50 ms, 80 ms, 120 ms and 200 ms. For each experiment, 512 scans were collected over 128 increments.

A series of sixteen ^{1}HN-R_2 ^{15}N-HSQC-IP experiments were recorded using a transfer INEPT period of 1.8 ms,

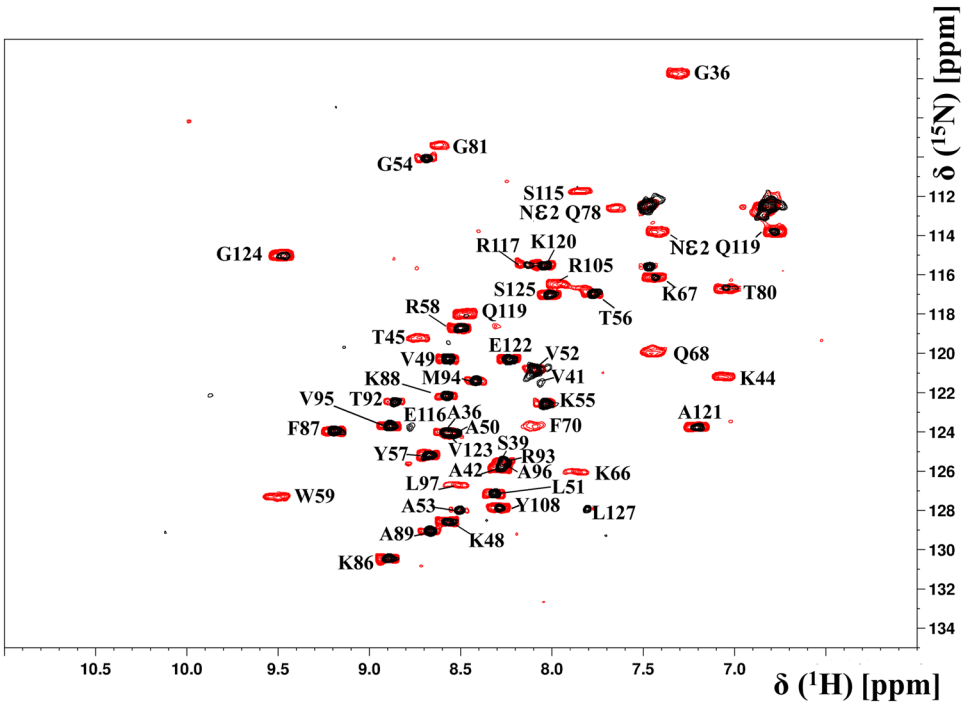

Fig. 1 Overlay of standard ^{15}N-HSQC (black) vs ^{15}N-HSQC-AP (red). The backbone assignment of the visible diamagnetic and paramagnetic resonances is reported

2.3 ms, 3 ms, 3.6 ms, 4.8 ms, 6 ms, 7.2 ms, 8.4 ms, 10.8 ms, 11.6 ms, 13.2 ms, 16 ms, 18 ms, 23.2 ms, 25.6 ms and 30.2 ms. For each experiment, 64 scans were collected over 156 increments.

A series of twelve ^{1}HN-R_2-weighted ^{15}N-HSQC-AP experiments was recorded, using INEPT transfer periods of 0.1 ms, 0.2 ms, 0.3 ms, 0.6 ms, 0.7 ms, 1.0 ms, 1.2 ms, 1.6 ms, 2.0 ms, 2.8 ms, 4.0 ms, 5.0 ms. For each experiment, 768 scans were collected over 128 increments.

Peaks were integrated using CARA software and the different relaxation rates were calculated using EXCEL/ORIGIN software.

Extent of assignment and data deposition

Paramagnetic relaxation

Standard NMR experiments allowed us the identification and the assignment of several sequential protein fragments: 37–39, 41–42, 48–58, 85–96, 116–117 and 120–127 (C-term). In the ^{15}N HSQC, this corresponded to only 37 HN signals out of 87 non-proline residues. Therefore, 59% of residues remained unassigned due the presence of two $[Fe_2S_2]^{+}$ clusters, which enhance the relaxation rates of spins nearby. The dipolar coupling between nuclear and electron spins gives a contribution to nuclear relaxation that is dependent on r^{-6}, where r is the distance between the two spins (Trindade et al. 2022). For a $[Fe_2S_2]^{+}$ cluster, the assumption that the electron spins can be considered as fully localized on the Fe ions is a reasonable approximation (Banci et al. 2018; Invernici et al. 2022; Machonkin et al. 2005; Trindade et al. 2021a). As a consequence, signals close to at least one of the four iron ions escape from sequential assignment. Predicting the extent of the radius of such "blind" sphere around an iron ion paramagnetic center is not straightforward (Trindade et al. 2020, 2021c); $[Fe_2S_2]^{+}$ is an antiferromagnetically coupled system in which the magnetic coupling gives rise to a new electron spin energy ladder and gives electronic correlation times that are different from that of the isolated ions (Bertini et al. 2016). In the case of CISD3, a sequential assignment shows that no signal can be assigned with standard experiments within a sphere of 9 Å from the closest iron ion (Lipper et al. 2018).

However, triple and double resonance, ^{13}C detected and also ^{1}H homonuclear experiments (Camponeschi et al. 2019) can be customized to minimize the loss of signal intensity and to optimize the efficiency of coherence transfer wherever the latter "competes" with relaxation (Invernici et al. 2020). Moreover, coherence transfer pathways and experiments may be re-designed according to the relaxation properties in order to make them more "robust" vis-à-vis with paramagnetic induced relaxation (Piccioli 2020). In CISD3, a ^{15}N HSQC-AP experiment showed eighteen more resonances, that were missing or very barely detectable in "routine" ^{15}N HSQC spectra as shown in Fig. 1.

The relative orientation of each backbone fragment with respect to the iron ions is such that a specific coherence transfer pathway may be marginally affected by paramagnetic relaxation while another one is affected more severely

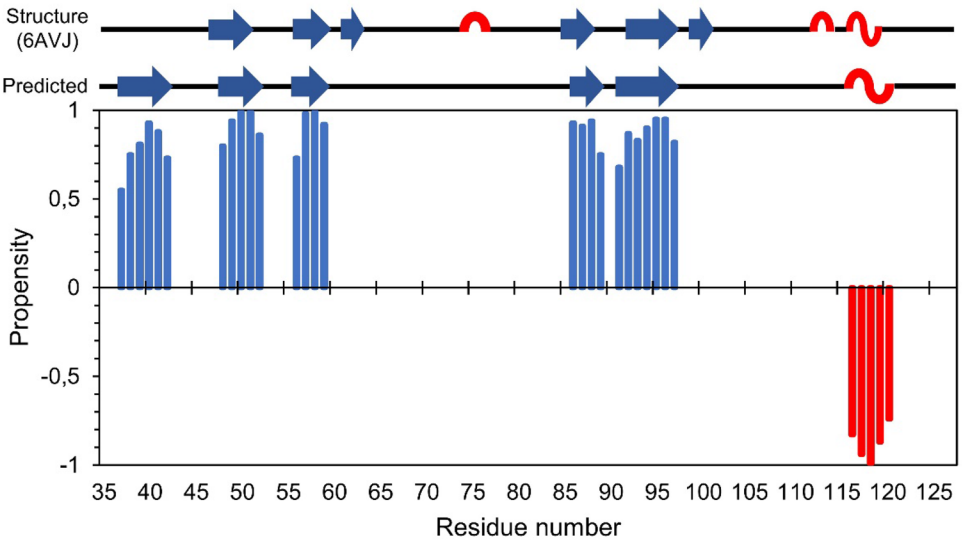

Fig. 2 Secondary structure prediction of CISD3 using TALOS (Shen et al. 2009). The black line represents the unstructured part of the protein, the blue arrows represent the β-strands and the red line the α-helix

(Trindade et al. 2020, 2021c). Therefore, to assign the eighteen HN resonances which are strongly affected by the paramagnetic centers, we had to devise a nonsystematic approach strategy. To extend the assignment of CISD3, we used R_1 and R_2 relaxation rates of the unassigned signals. Indeed, according to the r^{-6} relationship discussed above, paramagnetic relaxation rates can be converted into distances from the closest iron ion, like conventional ^{1}H-^{1}H NOEs (Bertini et al. 1997). Such distances were used, together with the scalar connectivities available from tailored experiments, to obtain the assignment. In turn, this procedure has also permitted to extend the assignment of ^{13}C signals that have been observed in the paramagnetic CON and CACO spectra but which could not be assigned due to the absence of sequential connectivities with assigned residues.

Overall, we identified the HN amide signals of residues 36, 44–45, 59, 66–68, 70, 80–81, 97, 105, 108, 115, 119, the two-proton sidechain belong to Q78 and Q119 and we extended the ^{13}C assignment for 65 residues. The blind region around the iron ions, that was initially 9 Å, has been decreased to 7 Å. The data deposited in BMRB cover the assignment of 51 HN backbone residues out of 87 non-proline resides, 65 Cα and 66 CO out of 93 expected resonances. Out of these, 15 HN-backbone, 21 Cα and 21 CO resonances arise from this approach. The protein's assignment has been deposited in the Biological Magnetic Resonance Data Bank (http://www.bmrb.wisc.edu) under the accession number 51439. The raw data of the experiments, both conventional triple resonance experiments and experiments optimized for the detection of fast relaxing signals, have also been deposited in BMRBig with the code: bmrbig82.

Secondary structure/paramagnetic shift

The hyperfine shift arises from the contact shift (scalar) and the pseudocontact shift (dipolar). FeS clusters have a very weak, if any, magnetic anisotropy, therefore the pseudocontact shifts do not contribute to the chemical shift of the nuclei. The contact shift is due to the electron delocalization from the metal ion via chemical bonds which is quenched by a few chemical bonds. As a consequence, in the case of $[Fe_2S_2]^+$ clusters, all signals affected by paramagnetic shifts fall within the blind sphere and are not detectable. Therefore, although incomplete, the analysis of the observed chemical shift is not affected by paramagnetism. Chemical shift values were hence used to predict the secondary structure using TALOS (Shen et al. 2009) and the data compared with the available X-ray structure (PDB code: 6AVJ) as shown in Fig. 2, with a good agreement for the assigned regions.

In the predicted secondary structure, two small β-strands and two small α-helices are missing. These features correspond to the missing assignments due to relaxation enhancement. The extra N-terminal β-strand is only present in the predicted secondary structure; however, a close inspection of the X-ray structure show that there are hints of β-strand propensity.

Conclusion

The partial assignment of this highly paramagnetic protein is an important step in the full characterization of CISD3. The presence of two Fe-S centers proved to be a challenge for the assignment. Future studies are necessary to understand the effect of histidine in the protein structure and to use NMR observables to refine the crystallographic structure of mutant

CISD3. However, although largely incomplete, this assignment offers the opportunity to monitor the protein structure/conformation and to address the interaction of CISD3 with small molecules or with protein partners, like its homologous protein CISD1 (Hou et al. 2007). In perspective, this may help to elucidate the possible role of CISD3 in cancer, diabetes and neurodegenerative diseases.

Acknowledgements The authors acknowledge the support by the Italian Ministry for University and Research (FOE funding) to the CERM/CIRMMP Italian Centre of Instruct-ERIC, a landmark ESFRI project. JMS acknowledges a Fellowship from TIMB3, Grant No. 810856, funded by the Horizon 2020 research and innovation program of the European Commission. DG is a PhD student supported under the EOSC-Life Project (ID:824087) funded by the Horizon 2020 EC program.

Author contributions JMS and MP wrote the manuscript, JMS and FC prepared figures; JMS, DG and FC performed the assignment; all authors reviewed the manuscript.

Data availability Assignment deposited in BMRB, ID 51439. Raw data deposited in BMRBig, ID bmrbig82.

Declarations

Competing interests The authors declare no competing financial interest.

References

Banci L, Camponeschi F, Ciofi-Baffoni S, Piccioli M (2018) The NMR contribution to protein-protein networking in Fe-S protein maturation. J Biol Inorg Chem 23:687. https://doi.org/10.1007/s00775-018-1552-x

Bermel W, Felli IC, Kümmerle R, Pierattelli R (2008) 13C direct-detection biomolecular NMR. Concepts Magn Resonance A 32A:183–200. https://doi.org/10.1002/cmr.a.20109

Bertini I, Donaire A, Luchinat C, Rosato A (1997) Paramagnetic relaxation as a tool for solution structure determination: *Clostridium pasterianum* ferredoxin as an example. Proteins Struct Funct Genet 29:348–358. https://doi.org/10.1002/(SICI)1097-0134(199711)29:3%3c348::AID-PROT8%3e3.0.CO;2-6

Bertini I, Jimenez B, Piccioli M (2005) 13C direct detected experiments: optimization for paramagnetic signals. J Magn Reson 174:125–132. https://doi.org/10.1016/j.jmr.2005.01.014

Bertini I, Luchinat C, Parigi G, Ravera E (2016) NMR of paramagnetic molecules: applications to metallobiomolecules and models, vol 2. Elsevier, Amsterdam

Camponeschi F, Muzzioli R, Ciofi-Baffoni S, Piccioli M, Banci L (2019) Paramagnetic 1H NMR spectroscopy to investigate the catalytic mechanism of radical S-adenosylmethionine enzymes. J Mol Biol 431:4514–4522. https://doi.org/10.1016/j.jmb.2019.08.018

Chen YF, Kao CH, Chen YT, Wang CH, Wu CY, Tsai CY, Liu FC, Yang CW, Wei YH, Hsu MT, Tsai SF, Tsai TF (2009) Cisd2 deficiency drives premature aging and causes mitochondria-mediated defects in mice. Genes Dev 23:1183–1194. https://doi.org/10.1101/gad.1779509

Ciofi-Baffoni S, Gallo A, Muzzioli R, Piccioli M (2014) The IR-(1)(5) N-HSQC-AP experiment: a new tool for NMR spectroscopy of paramagnetic molecules. J Biomol NMR 58:123–128. https://doi.org/10.1007/s10858-013-9810-2

Ferecatu I, Goncalves S, Golinelli-Cohen MP, Clemancey M, Martelli A, Riquier S, Guittet E, Latour JM, Puccio H, Drapier JC, Lescop E, Bouton C (2014) The diabetes drug target MitoNEET governs a novel trafficking pathway to rebuild an Fe-S cluster into cytosolic aconitase/iron regulatory protein 1. J Biol Chem 289:28070–28086. https://doi.org/10.1074/jbc.M114.548438

He QQ, Xiong LL, Liu F, He X, Feng GY, Shang FF, Xia QJ, Wang YC, Qiu DL, Luo CZ, Liu J, Wang TH (2016) MicroRNA-127 targeting of mitoNEET inhibits neurite outgrowth, induces cell apoptosis and contributes to physiological dysfunction after spinal cord transection. Sci Rep 6:35205. https://doi.org/10.1038/srep35205

Hou X, Liu R, Ross S, Smart EJ, Zhu H, Gong W (2007) Crystallographic studies of human MitoNEET. J Biol Chem 282:33242–33246. https://doi.org/10.1074/jbc.C700172200

Invernici M, Trindade IB, Cantini F, Louro RO, Piccioli M (2020) Measuring transverse relaxation in highly paramagnetic systems. J Biomol NMR 74:431–442. https://doi.org/10.1007/s10858-020-00334-w

Invernici M, Selvolini G, Silva JM, Marrazza G, Ciofi-Baffoni S, Piccioli M (2022) Interconversion between [2Fe-2S] and [4Fe-4S] cluster glutathione complexes. Chem Commun 58:3533–3536. https://doi.org/10.1039/d1cc03566e

Keller R (2004) The computer aided resonance assignment tutorial. pp 1–81

Kusminski CM, Holland WL, Sun K, Park J, Spurgin SB, Lin Y, Askew GR, Simcox JA, McClain DA, Li C, Scherer PE (2012) MitoNEET-driven alterations in adipocyte mitochondrial activity reveal a crucial adaptive process that preserves insulin sensitivity in obesity. Nat Med 18:1539–1549. https://doi.org/10.1038/nm.2899

Li Y, Wang X, Huang Z, Zhou Y, Xia J, Hu W, Wang X, Du J, Tong X, Wang Y (2021) CISD3 inhibition drives cystine-deprivation induced ferroptosis. Cell Death Dis 12:839. https://doi.org/10.1038/s41419-021-04128-2

Lipper CH, Karmi O, Sohn YS, Darash-Yahana M, Lammert H, Song L, Liu A, Mittler R, Nechushtai R, Onuchic JN, Jennings PA (2018) Structure of the human monomeric NEET protein MiNT and its role in regulating iron and reactive oxygen species in cancer cells. Proc Natl Acad Sci USA 115:272–277. https://doi.org/10.1073/pnas.1715842115

Machonkin TE, Westler WM, Markley JL (2005) Paramagnetic NMR spectroscopy and density functional calculations in the analysis of the geometric and electronic structures of iron–sulfur proteins. Inorg Chem 44:779–797. https://doi.org/10.1021/ic048624j

Mittler R, Darash-Yahana M, Sohn YS, Bai F, Song L, Cabantchik IZ, Jennings PA, Onuchic JN, Nechushtai R (2019) NEET proteins: a new link between iron metabolism, reactive oxygen species, and cancer. Antioxid Redox Signal 30:1083–1095. https://doi.org/10.1089/ars.2018.7502

Piccioli M (2020) Paramagnetic NMR spectroscopy is a tool to address reactivity, structure, and protein-protein interactions of metalloproteins: the case of iron–sulfur proteins. Magnetochemistry. https://doi.org/10.3390/magnetochemistry6040046

Salameh M, Riquier S, Guittet O, Huang ME, Vernis L, Lepoivre M, Golinelli-Cohen MP (2021) New insights of the NEET protein CISD2 reveals distinct features compared to its close mitochondrial homolog mitoNEET. Biomedicines. https://doi.org/10.3390/biomedicines9040384

Shen Y, Delaglio F, Cornilescu G, Bax A (2009) TALOS+: a hybrid method for predicting protein backbone torsion angles from NMR chemical shifts. J Biomol NMR 44:213–223. https://doi.org/10.1007/s10858-009-9333-z

Trindade IB, Invernici M, Cantini F, Louro RO, Piccioli M (2020) ^{1}H, ^{13}C and ^{15}N assignment of the paramagnetic high potential iron–sulfur protein (HiPIP) PioC from *Rhodopseudomonas palustris* TIE-1. Biomol NMR Assign 14:211–215. https://doi.org/10.1007/s12104-020-09947-6

Trindade IB, Hernandez G, Lebegue E, Barriere F, Cordeiro T, Piccioli M, Louro RO (2021a) Conjuring up a ghost: structural and functional characterization of FhuF, a ferric siderophore reductase from *E. coli*. J Biol Inorg Chem 26:313–326. https://doi.org/10.1007/s00775-021-01854-y

Trindade IB, Invernici M, Cantini F, Louro RO, Piccioli M (2021b) PRE-driven protein NMR structures: an alternative approach in highly paramagnetic systems. FEBS J 288:3010–3023. https://doi.org/10.1111/febs.15615

Trindade IB, Invernici M, Cantini F, Louro RO, Piccioli M (2021c) Sequence-specific assignments in NMR spectra of paramagnetic systems: a non-systematic approach. Inorg Chim Acta. https://doi.org/10.1016/j.ica.2020.119984

Trindade IB, Coelho A, Cantini F, Piccioli M, Louro RO (2022) NMR of paramagnetic metalloproteins in solution: Ubi venire, quo vadis? J Inorg Biochem 234:111871. https://doi.org/10.1016/j.jinorgbio.2022.111871